Journal of Controlled Release 356 (2023) 72–83

Contents lists available at ScienceDirect

Journal of Controlled Release

journal homepage: www.elsevier.com/locate/jconrel

RSPO3 Furin domain-conjugated liposomes for selective drug delivery to LGR5-high cells

Peter van Kerkhof [a,1], Tomica Kralj [a,1], Francesca Spanevello [a], Louis van Bloois [b], Ingrid Jordens [a], Jelte van der Vaart [a], Cara Jamieson [a], Alessandra Merenda [a], Enrico Mastrobattista [b,*], Madelon M. Maurice [a,*]

[a] Oncode Institute and Centre for Molecular Medicine, University Medical Centre Utrecht, Utrecht, the Netherlands
[b] Utrecht Institute for Pharmaceutical Sciences (UIPS), Utrecht University, Utrecht, the Netherlands

ARTICLE INFO

Keywords:
R-spondin-3
LGR5
Liposomes
Drug delivery
Doxorubicin
Cancer stem cells

ABSTRACT

The transmembrane receptor LGR5 potentiates Wnt/β-catenin signaling by binding both secreted R-spondin (RSPOs) and the Wnt tumor suppressors RNF43/ZNRF3, directing clearance of RNF43/ZNRF3 from the cell surface. Besides being widely used as a stem cell marker in various tissues, LGR5 is overexpressed in many types of malignancies, including colorectal cancer. Its expression characterizes a subpopulation of cancer cells that play a crucial role in tumor initiation, progression and cancer relapse, known as cancer stem cells (CSCs). For this reason, ongoing efforts are aimed at eradicating LGR5-positive CSCs.

Here, we engineered liposomes decorated with different RSPO proteins to specifically detect and target LGR5-positive cells. Using fluorescence-loaded liposomes, we show that conjugation of full-length RSPO1 to the liposomal surface mediates aspecific, LGR5-independent cellular uptake, largely mediated by heparan sulfate proteoglycan binding. By contrast, liposomes decorated only with the Furin (FuFu) domains of RSPO3 are taken up by cells in a highly specific, LGR5-dependent manner. Moreover, encapsulating doxorubicin in FuFuRSPO3 liposomes allowed us to selectively inhibit the growth of LGR5-high cells. Thus, FuFuRSPO3-coated liposomes allow for the selective detection and ablation of LGR5-high cells, providing a potential drug delivery system for LGR5-targeted anti-cancer strategies.

1. Introduction

The leucine-rich repeat-containing G protein–coupled receptor 5 (LGR5) belongs to a small family of seven-pass transmembrane proteins (LGR4/5/6) that are known to potentiate the Wnt/β-catenin signaling pathway [1–3] by binding R-spondin (RSPO) ligands and promote the internalization of the Wnt antagonists RNF43/ZNRF3 [4–8]. The RSPO family comprises four members of secreted proteins that contain two Furin-like repeats (Fu1 and Fu2), a Thrombospondin type 1 (TSP) domain, a basic region (BR) and a positively charged C-terminal region [9]. While the Fu1 and Fu2 domains are responsible for binding RNF43 and LGR5 respectively [6,11,12], the TSP/BR domain is known to interact with heparan sulfate proteoglycans (Fig. 1a) [13–15].

In healthy tissues, LGR4 is expressed in broad domains at low to moderate levels, while LGR5 and LGR6 expression patterns remain restricted to adult stem cell populations that require Wnt signaling for their homeostatic maintenance, e.g. in the gastrointestinal tract and skin [16–20]. Furthermore, LGR4–6 family members are frequently co-overexpressed in a variety of tumor types, including colorectal, ovarian and breast cancer and hepatocellular carcinoma [21–25]. In particular, high expression levels of LGR5 are linked to cancer stem cells (CSCs), a subpopulation of therapy-resistant cells that are able to refuel tumor growth [26]. In agreement, LGR5^{+} cells possess tumor-initiating properties [27], play a role in tumor progression [28,29] and are held responsible for cancer relapse [30,31]. While LGR5^{-} cells are capable to escape primary colorectal tumors and seed distant liver metastases, the outgrowth of metastatic lesions is dependent on the re-emergence of LGR5^{+} CSCs [32]. Consistently, specific ablation of LGR5^{+} CSCs

Abbreviations: RSPO, R-spondin; CSC, Cancer stem cell; LGR, Leucine-rich repeat-containing G protein-coupled receptor; Fu, Furin.

* Corresponding authors.
E-mail addresses: e.mastrobattista@uu.nl (E. Mastrobattista), m.m.maurice@umcutrecht.nl (M.M. Maurice).

[1] Equal contribution.

https://doi.org/10.1016/j.jconrel.2023.02.025
Received 2 September 2022; Received in revised form 15 February 2023; Accepted 17 February 2023
Available online 1 March 2023

strongly inhibits the development and maintenance of colorectal cancer metastasis, while primary tumor growth is halted temporarily [28,33].

The therapeutic need to neutralize CSCs has driven several efforts to develop LGR5-targeted cancer strategies over recent years [24,34]. Promising findings were reported for the application of LGR5 antibody-drug conjugates (ADC) that demonstrated tumor efficacy in xenotransplant mouse models for colorectal cancer [24,35]. Depending on the nature of the drug and targeted tissue, however, LGR5-ADC treatment may associate with gut toxicity due to on-target effects in healthy cells or local release of the conjugated drug [24].

An alternative strategy for effective drug delivery is the encapsulation of drugs in liposomal carriers [36]. Liposomal formulations are found to protect compounds from early inactivation, degradation and dilution in the circulation [37], thus offering improved pharmacokinetics while reducing systemic toxicity [38,39]. Furthermore, liposomes can be surface modified with targeting ligands, allowing for improved delivery to target cell populations with selectively increased expression of membrane receptors [40].

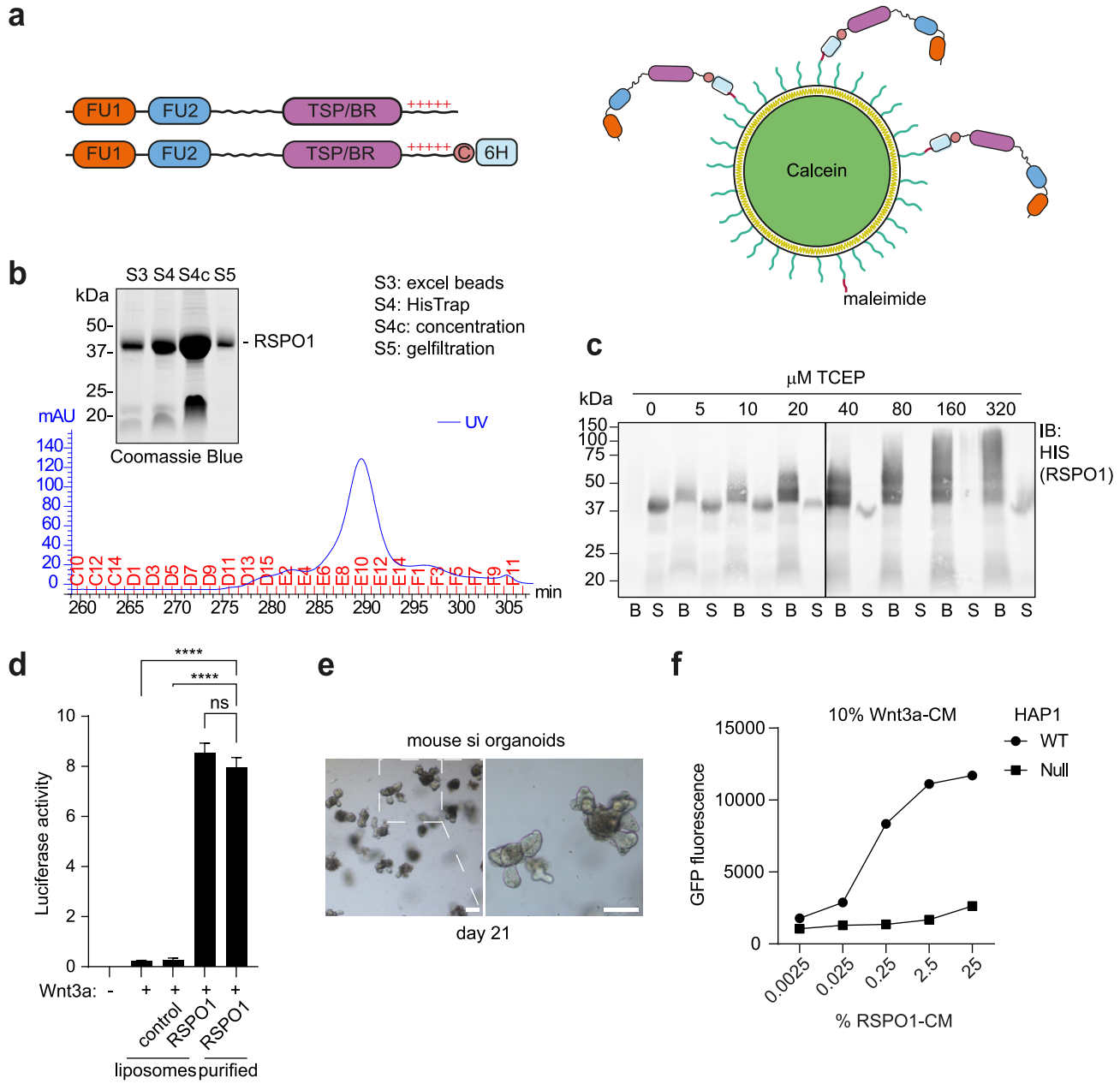

Fig. 1. Generation of functional RSPO1-coupled liposomes. (a) Schematic of full-length RSPO1 with an additional 6xHIS and Cys for its coupling to calcein-loaded liposomes via Maleimide. Fu, Furin; TSP/BR, thrombospondin/basic region; 6H, 6xHIS; C, cysteine. (b) Gel filtration elution pattern and Coomassie Blue staining of the multistep protein purification of RSPO1. (c) Coupling of RSPO1 to calcein-loaded liposomes in the presence of various TCEP concentrations. B, bound fraction; S, soluble fraction. (d) RSPO1-liposomes potentiate Wnt signaling comparable to purified RSPO1. Wnt luciferase reporter assay in HEK293T cells treated with 50 nM RSPO1-liposomes versus 50 nM purified RSPO1. Graph shows average luciferase reporter activities +/− SD. (e) RSPO1-liposomes support long term mouse small intestinal (si) organoid growth. Bright field images of organoids 21 days in culture and 3 days after passaging in the presence of RSPO1-liposomes. Right image shows zoom in of area indicated in left image. Scale bars, 25 µm. (f) RSPO1 does not potentiate Wnt signaling in HAP1 LGR4/5/6 KO (Null) cells. HAP1 WT and Null cells treated with increasing concentrations of RSPO1-conditioned medium (CM) in 10% Wnt3a-CM. Representative graph showing fluorescence of the TOP-GFP reporter measured by FACS ($n = 3$). **** ($p < 0.0001$), ns (non-significant). (For interpretation of the references to colour in this figure legend, the reader is referred to the web version of this article.)

Here, we employ the LGR-ligand RSPO to develop a liposome-based tool for targeting LGR5$^+$ cells. In contrast to an earlier report [34], our results show that full-length RSPO1-coupled liposomes are not suitable for targeting LGR5$^+$ cells, due to their prominent LGR5-independent uptake. The broad cellular uptake of RSPO1-liposomes is mediated by binding of the TSP/BR domain to heparan sulfate proteoglycans that are distributed ubiquitously on the surface of many cell types [41]. We overcome this issue by coupling RSPO3 Furin-like domains (FuFuRSPO3), which display high affinity to LGR5 [1], to the surface of liposomes and allow for specific recognition of LGR5-overexpressing cells. Lastly, we show that doxorubicin-loaded liposomes with FuFuRSPO3 coupled to the liposomal surface mediate selective depletion of LGR5-high expressing cells, including cancer cell lines (colorectal and liver) and Adenomatous Polyposis Coli (APC)-mutant small intestinal organoids, providing proof of concept for the development of LGR5$^+$ CSC-targeted treatment strategies.

2. Materials and methods

2.1. Plasmids and antibodies

RSPO1-6xHis-Cys, encoding the RSPO1 protein with a free cysteine at its C-terminus followed by a TEV site and a 6xHis tag, was subcloned into pcDNA4/TO by PCR using human RSPO1 cDNA (Source BioSciences) as a template. FuFuRSPO3-APEX2-V5-6xHis-Cys encodes for the Furin domains (amino acids 1–146) of human RSPO3 fused to the ascorbate peroxidase APEX2 (a kind gift from Marian Kalocsay, Harvard Medical School, Boston) for increased protein stability. The Fu1/2 domains of RSPO3 (DNA SU plasmid repository, amino acids 1–146) were subcloned via PCR and placed upstream of (GGSS)2-APEX2-V5 in pcDNA4/TO after which a double 6xHis-tag and a cysteine were added to the C-terminus of APEX2. Inducible N-terminal SNAP-tagged mature human LGR5 (iSNAP-LGR5) was generated by PCR-subcloning human LGR5 (kind gift of Hans Clevers, Hubrecht, Utrecht) behind a mouse H2-Kb signal sequence and a SNAP-tag in pcDNA4/TO [42]. All constructs were sequence verified. For immunoblot mouse anti-His (AD1.1.10; SantaCruz) was used in combination with goat anti-mouse Alexa^{680} (Invitrogen).

2.2. Cell and organoid cultures

Human Embryonic Kidney (HEK) 293T, iSNAP-LGR5 HEK293TR and Huh7 cells were cultured in DMEM high glucose (Invitrogen), respectively, supplemented with 10% fetal bovine serum (GE Healthcare), 2 mM UltraGlutamine (Lonza), 100 units/mL penicillin and 100 μg/mL streptomycin (Invitrogen). The medium for iSNAP-LGR5 HEK293TR cells contained Blasticidin (10 μg/mL) and Zeocin (100 μg/mL) to select for the Tet-R and the iSNAP-LGR5 plasmid. Wildtype mouse fibroblasts (MEFs) and Lgr4/5/6 triple knockout mouse fibroblast with SuperTopFlash (kind gift of Reversade lab) were cultured in MEMalpha with nucleosides (Gibco) supplemented with 10% fetal bovine serum (GE Healthcare), 100 units/mL penicillin and 100 μg/mL streptomycin (Invitrogen). HAP1-7TGP and HAP1-7TGP LGR4/5/6 triple knockout cells were grown in Iscove's Modified Dulbecco's Medium (IMDM) with L-Glutamin, with Hepes without Alpha-Thioglycerol (Gibco) supplemented with 10% fetal bovine serum (GE Healthcare), 100 units/mL penicillin and 100 μg/mL streptomycin (Invitrogen). LoVo cells were cultured in DMEM/F12 with Glutamine (Gibco) supplemented with 10% fetal bovine serum (GE Healthcare), 100 units/mL penicillin, 100 μg/mL streptomycin (Invitrogen) and 1 mM Sodium Pyruvate (Gibco). All cells were cultured at 37 °C in 5% CO2. Wnt3a-conditioned medium (CM) was obtained from L-cells stably expressing and secreting Wnt3a [43] cultured in DMEM low glucose (Invitrogen). RSPO- and Noggin-CM were produced as described before [44]. For β-catenin-mediated reporter assays, cells were stimulated overnight (o/n). Transfections were performed using either FuGENE 6 (Promega) according to manufacturer's protocol for β-catenin-mediated reporter assays and microscopy or polyethylenimine (PEI) for protein expression.

Small intestinal C57BL/6 mouse organoids (kindly provided by Bon-Kyoung Koo, IMBA, Austria) were cultured in matrigel (Corning) or BME (Cultrex, 3536–005-02) drops in AdvDMEM+++ (Advanced DMEM/F12 medium (Invitrogen) supplemented with 0.01 M Hepes (Gibco), 1× GlutaMAX (Gibco), 100 U/mL penicillin, 100 μg/mL streptomycin)with 5% human RSPO1 CM (corresponding to 370 ng/mL RSPO1), 100 ng/mL recombinant murine Noggin (PeproTech, UK) or 2.5% human Noggin CM, 50 ng/mL recombinant murine EGF (Gibco), 1× B-27 supplement (Invitrogen), 1× N-2 supplement (Invitrogen), 1.25 mM n-Acetyl Cysteine (Sigma-Aldrich) (AdvDMEM+++). To assess the ability of liposomal RSPO1 to support organoid growth, organoid cultures were split and RSPO1-conditioned medium was replaced with an equivalent amount of liposome-coupled RSPO1 or purified protein, as a control. APC-mutant organoids were generated from small intestinal C57BL/6 mouse organoids using CRISPR-Cas9 targeting exon 15 to create the homozygous Y620LfsX630 mutation.

2.3. Recombinant human RSPO1 and FuFuRSPO3APEX expression and purification

Recombinant human RSPO1 or FuFuRSPO3APEX was produced in HEK293T cells grown in a cell factory (2528 cm^2 culture area, Thermo Fisher Scientific) and transfected with 275 μg RSPO1- or FuFuRSPO3APEX-encoding plasmids by using PEI. After six hours, the medium was replaced with Advanced DMEM/F12 medium supplemented with 0.01 M Hepes, 1× GlutaMAX, 100 U/mL penicillin, 100 μg/mL streptomycin to allow RSPO secretion in a low protein medium to facilitate the purification. Supernatant was harvested four days after transfection, cleared by centrifugation and stored at 4 °C.

RSPO was purified using a two-step immobilized metal ion affinity chromatography (IMAC) procedure. First, the supernatant was incubated o/n at 4 °C with Ni Sepharose excel beads (GE Healthcare). The next day, RSPO-bound excel beads were harvested by low-speed centrifugation, packed into a Tricorn chromatography column and placed in the AKTA-purifier system (Amersham Biosciences). The column was equilibrated with buffer A (500 mM NaCl, 20 mM Hepes, pH 7.5), washed with 15 mM imidazole in buffer A and bound proteins were eluted in 1 mL fractions using 300 mM imidazole in buffer A for 20 min at 1 mL/min. Peak fractions were determined by SDS-PAGE and Coomassie staining. Peak fractions were pooled and diluted to 50 mL with buffer A, leading to a final imidazole concentration of 36 mM. This sample was loaded on an equilibrated 1 mL HisTrap HP column (GE Healthcare) using the AKTA system and bound proteins were eluted in 0.5 mL fractions using two linear gradients of 1 M imidazole in buffer A, 0–1% for 10 min followed by 1–50% for 20 min both at a flow rate of 0.5 mL/min. Peaks fractions were analysed by SDS-PAGE and Coomassie staining to assess purity and apparent MW. For RSPO1 purification, peak fractions were pooled and concentrated using Vivaspin 20 concentrators (MWCO 3 kDa, GE Healthcare) to 0.5 mL. This was subsequently applied to a Superdex200 10/300 gelfiltration column to separate full length protein from a smaller degradation product. Proteins were eluted in 0.5 mL fractions in Hepes buffered saline (HBS) (10 mM HEPES pH 7.5, 136 mM NaCl). Peak fractions of the first elution peak were pooled and concentrated to 1 mL. The final purified protein was aliquoted and stored at −80 °C in low protein binding tubes (Eppendorf). Concentrations of purified RSPOs were estimated by comparison to a standard bovine serum albumin (BSA) curve using SDS PAGE and Coomassie staining. Coomassie stained protein was imaged using the Amersham Typhoon NIR laser scanner and quantified using Image Quant TL software V8.1 (Cytiva).

2.4. Preparation of liposomal RSPO

Liposomes containing DMPC (1,2-dimyristoyl-sn-glycero-3-

phosphocholine) or DPPC (1,2-dipalmitoyl-sn-glycero-3-phosphocholine), DSPE-PEG(2000) (1,2-distearoyl-sn-glycero-3-phosphoethanolamine-N-[amino(polyethylene glycol)-2000] (ammonium salt), DSPE-PEG(2000) Maleimide (1,2-distearoyl-sn-glycero-3-phosphoethanolamine-N-[maleimide(polyethylene glycol)-2000] (ammonium salt), and cholesterol at a 20:1.6:0.4:20 M ratio were prepared by the lipid film hydration and extrusion method [45]. Briefly, lipids were dissolved in $CHCl_3$/MeOH (1:1 (v/v) ratio) in a round bottom flask and solvent was evaporated using a rotary evaporator device. The formed lipid film was further dried under a stream of nitrogen to remove traces of organic solvent.

To obtain calcein-loaded liposomes, the thin lipid film was hydrated with 75 mM calcein solution in Hepes pH 7, containing 10 mM EDTA by vigorously vortexing in the presence of glass beads. The formed multilammelar liposomes were subsequently extruded through polycarbonate filters with pore sizes varying from 0.1 to 0.2 μm using a hand extruder (Avanti Polar Lipids) to obtain unilamellar vesicles in the size range of 100–250 nm. Liposomes were then pelleted by ultracentrifugation (100.000 ×*g*, 1 h, RT) and washed three times by centrifugation and resuspended in HBS with 10 mM EDTA. For RSPO coupling, purified proteins were mixed with liposomes and incubated for 1 h at RT followed by o/n incubation at 4 °C. After coupling, liposomes were centrifuged for 1 h at 100.000 ×g at 4 °C (Beckman Optima TL, TLA45 rotor). Liposomes were washed twice with 1 mL HBS to remove free calcein and unbound RSPO. Lastly, liposomes were resuspended in 1 volume of HBS. To obtain doxorubicin-loaded liposomes an ammonium sulfate gradient was used [46]. Briefly, the lipid film was resuspended in 240 mM $(NH_4)_2SO_4$, 1 mM EDTA. The formed liposomes were extruded, pelleted and resuspended as described above. Next, purified RSPO was directly mixed with liposomes at 15 μg/mL and incubated for 1 h at 37 °C. The liposome RSPO mixture was diluted with 1 volume doxorubicin (1 mg/mL) and incubated for 2 h at 37 °C followed by o/n incubation at 4 °C. The next day, liposomes were centrifuged for 1 h at 100.000 ×g at 4 °C and washed twice with 1 mL HBS to remove free doxorubicin and unbound RSPO. Finally, liposomes were resuspended in 1 volume of HBS.

2.5. Liposome characterization

The final concentration of liposomes was determined by phosphate analysis according to Rouser et al. [47]. The average size distribution of the various liposome batches was determined by Dynamic Light Scattering (DLS) using 20 μL liposomes diluted in 3 mL 10 mM Hepes pH 7. 1 mL of diluted liposome suspension was transferred to a quartz batch cuvette (Malvern, UK) and measured on a Malvern Zetasizer Nano ZS. The zeta potential was determined by Phase analysis light scattering (PALS). To this extent, liposomes were diluted 1:150 in 10 mM Hepes pH 7 and transferred to a Malvern cuvette with electrode. Zeta potential was measured on a Malvern Zetasizer Nano ZS instrument. Liposomal calcein concentrations were determined on a Nanodrop ND-1000 spectrophotometer (Thermo Scientific) at 495 nm and calculated based on the extinction coefficient of 18,258 M^{-1} cm-1 [48]. Liposomal doxorubicin concentration was determined after adding 0,1 volume of 10% TX100 and measuring the absorbance at 480 nm on a Nanodrop ND-1000 spectrophotometer using a standard curve of doxorubicin. Measured values are included in Supplemental Table 1. For viability assays, liposome concentrations were equalized based on phosphate content.

2.6. Western blotting

Western blotting was performed using standard procedures with Immobilon-FL PVDF membranes (Millipore). In short: after protein transfer, the membranes were blocked for 1 h at RT in 1:1 ratio Odyssey blocking buffer (LI-COR): PBS. Primary antibodies were incubated o/n at 4 °C and secondary antibodies for 1 h at RT in the dark in PBS with 0.1% Tween 20. The Typhoon (GE Healthcare) infrared imaging system was used for immunoblot analysis.

2.7. β-catenin-mediated reporter assays

HEK293T cells were seeded in 24-well plates and transfected the next day with 30 ng of reporter construct TOPFlash and 5 ng of thymidine kinase (TK)-Renilla. Cells were stimulated 6 h post-transfection with Wnt3a-CM and RSPO-CM or RSPO-liposomes o/n, then cells were lysed in Passive lysis buffer (Promega) for 20 min at RT. Levels of Firefly and Renilla luciferase were measured using the Dual Luciferase Kit (Promega) according to the manufacturer's instructions on a Berthold luminometer Centro LB960. Bar graphs and dose-response curves were made using Prism 9.5.0 (Graphpad).

2.8. Confocal microscopy and SNAP labeling

iSNAP-LGR5 HEK293TR cells were grown on laminin-coated glass coverslips and HAP1 or MEF cells on non-coated glass coverslips in 24-well plates. Doxycycline was added iSNAP-LGR5 HEK293TR cells at a concentration of 0,5 μg/mL to induce LGR5 overexpression. Next day, medium was replaced with 250 μL medium with calcein- or doxorubicin-loaded RSPO-liposomes. Heparin or excess of purified RSPO was added as indicated in figure legends. Calcein- or doxorubicin-loaded liposomes without coupled RSPO were used as background control. For SNAP labeling, cells were labeled with 1 μM SNAP-surface-Alexa^{549} or SNAP-surface-Alexa^{647} (New England Biolabs). Uptake of liposomes and SNAP-surface-Alexa^{549} was allowed for 3 h at 37 °C after which cells were washed with warm medium and fixed in 4% paraformaldehyde in 0,1 M Sodium Phosphate buffer pH 7.4 for 30 min at RT. Fixative was quenched for 10 min at RT with 20 mM NH_4Cl. Cells were labeled with 0,2 μg/mL DAPI and 2 μg/mL Phalloidin-Alexa^{647} (Invitrogen) in PBS for 30 min at RT, washed in water, mounted in ProLong Gold (Life Technologies) and visualized using a Zeiss LSM700 confocal microscope. ImageJ was used to process the images.

2.9. FACS

To measure uptake of calcein-loaded RSPO-liposomes in iSNAP-LGR5 HEK293TR, HAP1-7TGP or HAP1 Lgr4/5/6 KO cells, cells were seeded in 24 wells plates at a density of 2×10^5 cells/well. iSNAP-LGR5 HEK293TR cells were treated with 0,5 μg/mL doxycycline to induce LGR5 overexpression. Next day, cells were incubated with the indicated liposomes for 4 h at 37 °C. During the incubation, heparin (Sigma-Aldrich) or excess purified RSPO protein was added as indicated in figure legends. Data was analysed using FlowJo v10. For SNAP-surface labelling of SNAP-LGR5 expressing HEK cells, 1 μM SNAP-Surface-Alexa^{549} (NEB) was added during the last 10 min of incubation at 37 °C. Cells were harvested in 100 μL 0,05% Trypsin-EDTA solution in PBS and diluted with 500 μL 1% BSA in PBS. Cells were collected by centrifugation for 3 min at 300 ×*g* and resuspended in 500 μL 1% BSA in PBS. Calcein fluorescence of 10.000 singlet-gated cells was measured by FACS on a BD Celesta Flow cytometer (BD Biosciences) using a 488 laser and 530/30 BP filter. SNAP^{549} was measured using a 561 nm laser combined with a 585/15 BP filter. The mean Fluorescence of the gated population is depicted in the graphs. Dose response curves were made using Prism 9.5.0 (Graphpad).

2.10. Cell viability assays

iSNAP-LGR5 HEK293TR, Huh7 and LoVo cells were seeded in 24 wells plates at a density of 20×10^3 cells/well in 1 mL. To induce overexpression of LGR5, 0,5 μg/mL doxycycline was added to the iSNAP-LGR5 HEK293TR cells. Next day, medium was replaced with 300 μL medium containing doxorubicin or doxorubicin-loaded RSPO-liposomes as indicated in the figures or figure legends. For Huh7 and LoVo

cells, liposomes loaded with highest concentrations of doxorubicin were used. Cells were incubated for 3 h at 37 °C with liposomes containing the indicated doxorubicin concentration used in a 1:800 dilution. Subsequently the medium was replaced with 1 mL normal growth medium. Cells were incubated for 6 days at 37 °C, fixed with 100% methanol and stained with 0,5% Crystal violet in 25% methanol. Plates were scanned using the Amersham Typhoon NIR laser scanner and quantified and processed using ImageJ. To assess sensitivity of APC-mutant (APC^{mut}) and wild-type (WT) organoids to doxorubicin-loaded FuFuRSPO3-coupled liposomes, organoids were cultured in WENR-medium (AdvDMEM+++, 5% human RSPO1 CM, 2.5% human Noggin CM, 50 ng/mL recombinant murine EGF (Gibco), 0.5 nM Wnt Surrogate [49], 1× B-27 supplement (Invitrogen), 1× N-2 supplement (Invitrogen), 1,25 mM n-Acetyl Cysteine (Sigma-Aldrich) for at least one passage. Organoids were then mechanically sheared and seeded in 20 μL BME (Cultrex, 3536–005-02) droplets per well. Organoids were grown for 2–3 days in 250 μL WENR-medium. Medium was removed and replaced with 200 μL WENR-medium without RSPO1 CM supplemented with the indicated liposome dilutions or free doxorubicin and incubated for 2 h. Organoids were washed with 500 μL AdvDMEM+++ and subsequently grown in 250 μL WENR-medium. Medium was replaced every 2 days. Cell viability was determined after a 48 h chase using CellTiter-Glo® Luminescent Cell Viability Assay (Promega, G7570). In short, medium was removed and BME droplets were resuspended in 100 μL AdvDMEM+++. 100 μL of CellTiter-Glo® solution was added and incubated for 20 min at RT. 180 μL of the suspension was transferred to a white flat bottom 96 well assay plate and measured on a Berthold luminometer Centro LB960 according to manufacturer's protocol. Bar graphs were made using Prism 9.5.0 (Graphpad).

2.11. Reverse transcription and quantitative real-time PCR

To determine expression values of RSPO binding partners in APC^{mut} and WT organoids, RNA from three wells of independently grown organoids was extracted using RNeasy Mini kit (Qiagen) according to manufacturer's protocol. 500 ng of total RNA was processed to cDNA using iScript cDNA Synthesis kit (Biorad, #1708891) according to manufacturer's protocol. The synthesized cDNA was subsequently used in a qRT–PCR using IQ SYBR green mix (Biorad, #1708886) according to manufacturer's protocol. A similar protocol was used to determine LGR5 expression in HEK293T, Huh7 and LoVo cells. The primer pairs used for the qRT-PCR are listed in Supplementary Table 2. Bar graphs were made using Prism 9.5.0 (Graphpad).

2.12. Statistics

Statistical analysis was determined by One- or Two-way Anova using Prism 9.5.0 (Graphpad). Statistical details are specified in the figure legends were applicable.

3. Results

3.1. Generation of functional RSPO1-coupled liposomes

To conjugate full-length human RSPO1 to the liposomal surface, we prepared liposomes using 1,2-dimyristoyl-sn-glycero-3-phosphatidylcholine (DMPC), cholesterol, and 1,2-distearoyl-sn-glycero-3-phosphorylethanolamine(DSPE)-PEG2000 in a 20:20:2 ratio. PEGylated phospholipids were incorporated to prevent aspecific binding of liposomes to cells [50]. To allow for coupling of RSPO1 to the distal terminus, we replaced 20% of DSPE-PEG2000 with maleimide-functionalized DSPE-PEG2000 phospholipids that are reactive to free sulfhydryl groups [51,52]. According to the available RSPO1 crystal structure, all 16 Cys residues present in the two Furin-like domains form disulphide bonds in the native structure of the protein and thus will not provide maleimide-reactive free thiols [6]. Similarly, the RSPO C-terminal TSP/BR domain carries 6 Cys residues that also form disulphide bridges [53]. Therefore, to introduce a free thiol group, we modified wild-type RSPO1 by adding an additional Cys residue at its C-terminus. In addition, to facilitate purification of the recombinant protein a 6xHis tag was added (Fig. 1a). After a three-step affinity chromatography purification (Fig. 1b), optimal coupling efficiency of recombinant RSPO1 to liposomes was achieved by adding 25 μM of the reducing agent TCEP (Fig. 1c, S1a). Covalent coupling was exemplified by a visible shift in molecular weight of RSPO1, when comparing soluble and liposome-bound fractions (Fig. 1c, S1b). Furthermore, RSPO1-coupled liposomes formed a stable suspension of monodisperse particles. To visualize and quantify the uptake of liposomes into cells, RSPO1-conjugated and control liposomes were loaded with 75 mM calcein, a fluorescent compound that is self-quenching at high concentrations (Fig. 1a) [54]. Uptake of RSPO-liposomes, which may be mediated either by endocytosis or by fusion with the plasma membrane [55], will lead to release of the dye and activation of its fluorescent properties [55].

Next, we assessed whether the introduced modifications and liposome coupling affected the biological activity of RSPO1 as compared to purified wild-type RSPO1. Using a β-catenin-dependent luciferase reporter assay [56], we observed that RSPO1-liposomes displayed similar Wnt-potentiating activity in HEK293T cells as purified RSPO1, indicating that RSPO1-liposomes fully retain functional activity (Fig. 1d). Furthermore, RSPO1-coupled liposomes were well able to support the growth of murine small intestinal organoids, confirming their ability to enhance endogenous Wnt/β-catenin signaling (Fig. 1e). Notably, the response of cells to RSPO1 was strictly LGR-dependent, as no Wnt potentiation was observed in *LGR4/5/6* knockout HAP1 cells that carry a stably integrated β-catenin-dependent GFP reporter (Fig. 1f), as shown previously[55].

Thus, functionalized liposomes decorated with purified recombinant full-length RSPO1 retain essential functional properties of endogenous LGR ligands.

3.2. Cellular uptake of RSPO1-coupled liposomes is largely LGR5-independent

After confirming their LGR-dependent biological activity, we sought to address binding specificity of calcein-loaded RSPO1-liposomes to their cognate receptors at the cell surface. To address this issue, we first evaluated the uptake of unconjugated and RSPO1-coupled liposomes in HEK293T cells by immunofluorescence and flow cytometry analysis in the presence and absence of excess purified RSPO1 protein. Internalization of RSPO1-coupled liposomes was readily observed as indicated by acquired fluorescence within endocytic compartments (Fig. 2a), while uptake of unconjugated calcein-loaded liposomes was negligible (Fig. 2a). Addition of excess purified RSPO1 prevented binding of fluorescent RSPO1-coupled liposomes (Fig. 2a, b), indicating that the observed uptake is indeed RSPO1-mediated and not due to aspecific internalization or calcein leakage from liposomes.

To evaluate levels of LGR5-dependent uptake of RSPO1-coupled liposomes, we generated HEK293T cells that allow for doxycycline-inducible LGR5 overexpression. Again, uninduced cells displayed internalization RSPO1-coupled liposomes. Unexpectedly, levels of uptake were only increased slightly when LGR5 was overexpressed (Fig. 2c, d). These findings thus argue that prominent internalization of RSPO1-liposomes occurs regardless of LGR5 overexpression, raising doubts on their LGR5 selectivity.

To determine the relative role of LGR family members in RSPO1-dependent liposomal uptake, we incubated both wild-type and *LGR4/5/6* triple knockout HAP1 cells with calcein-loaded RSPO1 liposomes for 3 h. Strikingly, levels of internalization were comparable for wild-type and mutant cells (Fig. 2e). Similar observations were done in *LGR4/5/6* triple knockout MEF cells (Fig. S2a), indicating RSPO1-liposomes are internalized independent of LGRs. Given that the TSP/BR domain of

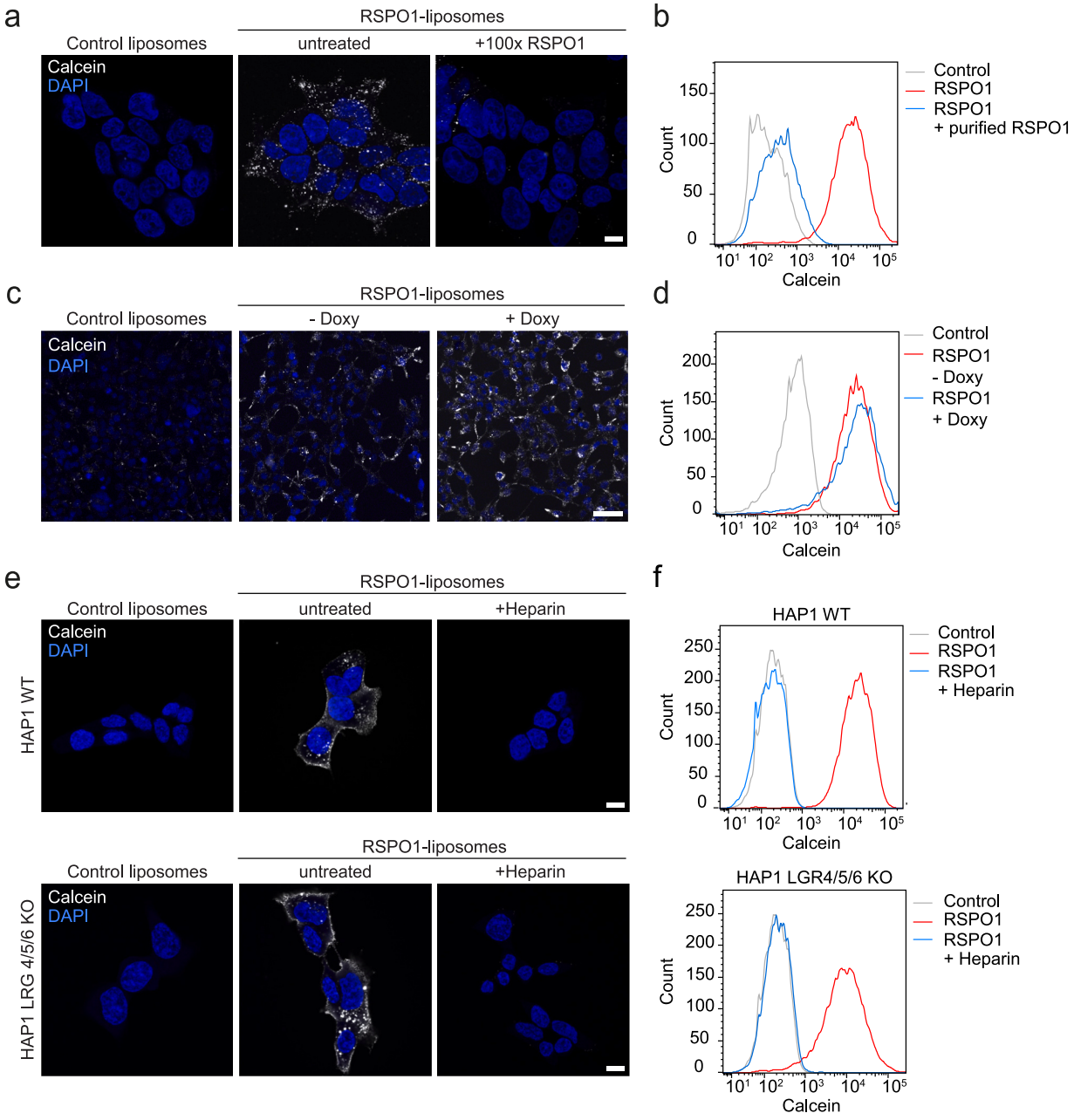

Fig. 2. RSPO1-liposomes cannot specifically detect LGR-positive cells. (a,b) Uptake of RSPO1-liposomes can be competed with purified RSPO1. Confocal images (a) and FACS plots (b) showing a 4 h uptake of calcein-labeled RSPO1-liposomes in HEK293T cells in the presence and absence of 100-fold excess purified RSPO1. Scale bar, 10 μm. (c,d) Uptake of RSPO1-liposomes is enhanced upon overexpression of LGR5. Confocal images (c) and FACS plots (d) showing the 4 h uptake of calcein-labeled RSPO1-liposomes in HEK293T cells in the presence (+Doxy) and absence (-Doxy) of LGR5 overexpression. Scale bar, 50 μm. (e,f) Uptake of RSPO1-liposomes is largely independent of LGRs. Confocal images (e) and FACS plots (f) showing a 3 h uptake of RSPO1-liposomes in HAP1 WT and LGR4/5/6 KO cells in the presence and absence of heparin (0,5 mg/mL). Scale bars, 10 μm.

RSPO family members interacts with heparan sulfate proteoglycans [13–15], we hypothesized that this activity may explain the LGR-independent internalization of RSPO1-coupled liposomes. Indeed, the uptake of RSPO1-liposomes was strongly inhibited by supplementation with heparin in concentrations above 100 nM both in wild-type cells and LGR KO cells (Fig. 2, e, f, S2b, S2c), thus confirming the engagement of heparan sulfate proteoglycans as the primary pathway for cellular uptake. These findings are in agreement with a recent study in which heparan sulfate proteoglycans were found to act as RSPO co-receptors and even may potentiate Wnt signaling in an LGR-independent manner [58].

Taken together, our findings clearly indicate that coupling full-length RSPO1 to liposomes does not allow for specific targeting of LGR5$^+$ cells, due to prominent proteoglycan-dependent internalization. Thus, uptake of RSPO1 does not correlate with LGR expression, even though the functional response to RSPO1 treatment is strictly LGR-dependent (Fig. 1f) [57]. Our findings thus challenge a previous study in which RSPO1-liposomes are used to target LGR5$^+$ cells [34] and point out that a more refined strategy is required for specific recognition and targeting of LGR5$^+$ cells.

3.3. FuFuRSPO3-coupled liposomes recapitulate RSPO3 biological activity

To overcome the limitations of using full-length RSPO and generate a LGR5-specific targeting tool, we decided to employ the Furin-like domains of RSPO3, that display a strongly increased binding affinity (up to 50-fold) for LGR5 when compared to LGR4 [1]. We engineered a Furin1-Furin2 fragment of RSPO3 (FuFuRSPO3) modified with a 6xHis-tag and an extra Cys residue at its C-terminus to perform purification and coupling procedures as shown for full-length RSPO1 (Fig. 1a, 3a, b). As the isolated FuFuRSPO3 fragment proved unstable in our hands, we added a well-folded domain (APEX2) to replace the TSP region which promoted stability of the recombinant protein (Fig. 3a). Again, we employed a thiol-maleimide reaction to generate fluorescent FuFuRSPO3-coupled liposomes. Coupling efficiency of the FuFuRSPO3 fragment to liposomes was less efficient than full-length RSPO1 (Fig. 3c) and was not improved by supplementation with TCEP (Fig. S3a). Nevertheless, FuFuRSPO3-coated liposomes were well able to potentiate Wnt signaling (Fig. 3d, S3b). Thus, FuFuRSPO3 displays preserved biological activity when coupled to liposomes.

3.4. Cellular uptake of FuFuRSPO3-coupled liposomes is LGR5-dependent

To assess LGR5-dependent cellular binding and uptake of calcein-loaded FuFuRSPO3-liposomes, we employed LGR5-inducible HEK293T cells. While FuFuRSPO3-liposomes weakly labeled untreated HEK293T cells in comparison to control liposomes, their uptake was strongly increased upon doxycycline-induced LGR5 expression, as revealed by flow cytometry (Fig. 4a).

Furthermore, FuFuRSPO3-liposomes were internalized in endocytic vesicles in LGR5-high cells (Fig. S4a). The increased uptake of FuFuRSPO3-liposomes mediated by high LGR5 expression was prevented by supplementation with excess recombinant FuFuRSPO3 protein, indicating that binding occurred in a FuFuRSPO3-specific manner (Fig. 4b, Fig. S4a).

Strikingly, and unlike RSPO1-coupled liposomes, the cellular uptake of FuFuRSPO3-liposomes could not be competed by heparin, indicating that binding does not occur via heparan sulfate proteoglycans and is LGR5-specific (Fig. 4c and d). In agreement with these findings, the uptake of FuFuRSPO3 displayed a strong correlation with LGR5 protein levels expressed at the cell surface, while this correlation was weak for RSPO1-liposomes (Fig. S4b). Together, these results demonstrate that binding and internalization of FuFuRSPO3-liposomes is dependent on the level of LGR5-expression at the cell surface.

3.5. Doxorubicin-loaded FuFuRSPO3-liposomes mediate selective killing of LGR5 high-expressing cells

We next investigated the possibility to employ FuFuRSPO3-liposomes for the selective delivery of drugs to cells that express high levels of LGR5. To this end, we employed the chemotherapeutic and DNA intercalating agent doxorubicin, for which physicochemical properties permit high drug entrapment and easy remote loading in pre-formulated liposomes [46]. We monitored cellular uptake and levels of chromatin binding of doxorubicin by utilizing its intrinsic fluorescent properties [59]. We noted that doxorubicin-loaded DMPC liposomes induced high levels of nuclear doxorubicin accumulation and cell death in target cells in an RSPO-independent manner (Fig. S5a), indicating that doxorubicin leakage prevented these liposomal formulations to be used for selective drug delivery [60,61]. To lower the rate of non-specific drug release, we switched to the usage of more stable C16 fatty acid-containing 1,2-dipalmitoyl-sn-glycero-3-phosphocholine (DPPC) liposomal formulations [62]. Treatment of LGR5-expressing HEK293T cells with doxorubicin-loaded FuFuRSPO3-coated DPPC liposomes for 3 h led to specific doxorubicin uptake, as shown by the accumulation of fluorescence in endosomal-like compartments and the

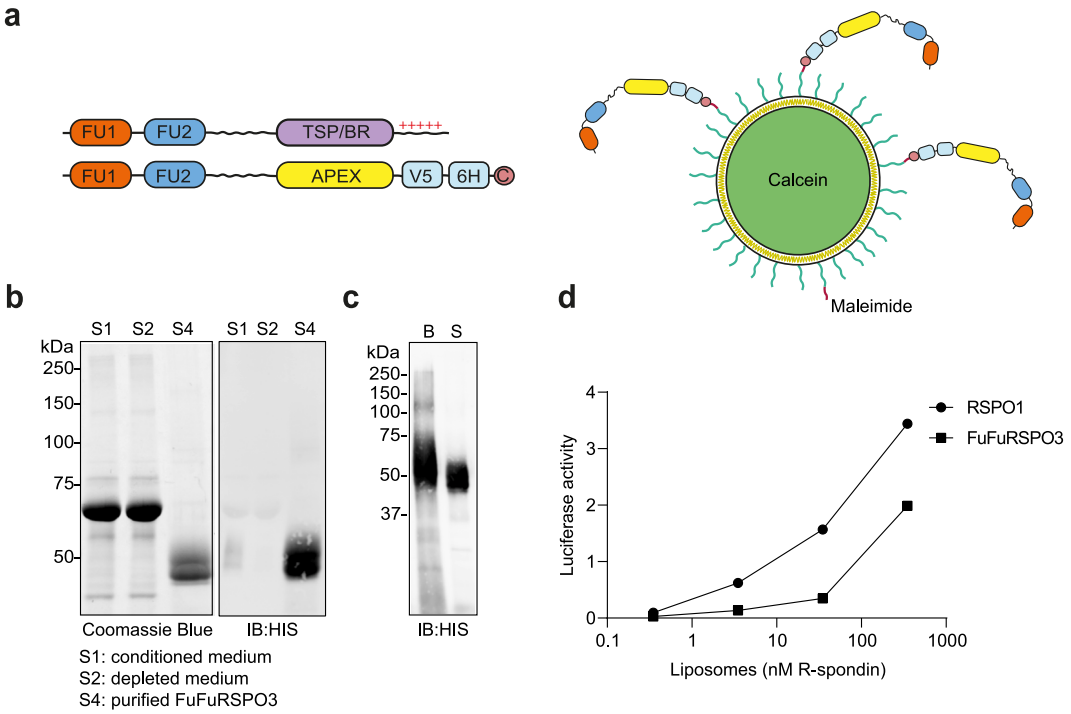

Fig. 3. Generation of functional RSPO3-coupled liposomes. (a) Schematic of full-length RSPO3 and FuFuRSPO3 with an APEX tag and an additional 6xHIS and a Cys for the coupling to calcein-loaded liposomes via maleimide. Fu, Furin; TSP/BR, thrombospondin/basic region; 6H, 6xHIS; C, cysteine. (b) Western blot and Coomassie Blue staining of the multistep protein purification of FuFuRSPO3. (c) Coupling of FuFuRSPO3 to calcein-loaded liposomes. B, bound fraction; S, soluble fraction. (d) FuFuRSPO3-liposomes can potentiate Wnt signaling. Wnt luciferase reporter assay in HEK293T cells treated with FuFuRSPO3-liposomes versus RSPO1-liposomes (nM) in 10% Wnt3a-CM. Graph shows a representative dose-response curve of luciferase reporter activities ($n = 2$). (For interpretation of the references to colour in this figure legend, the reader is referred to the web version of this article.)

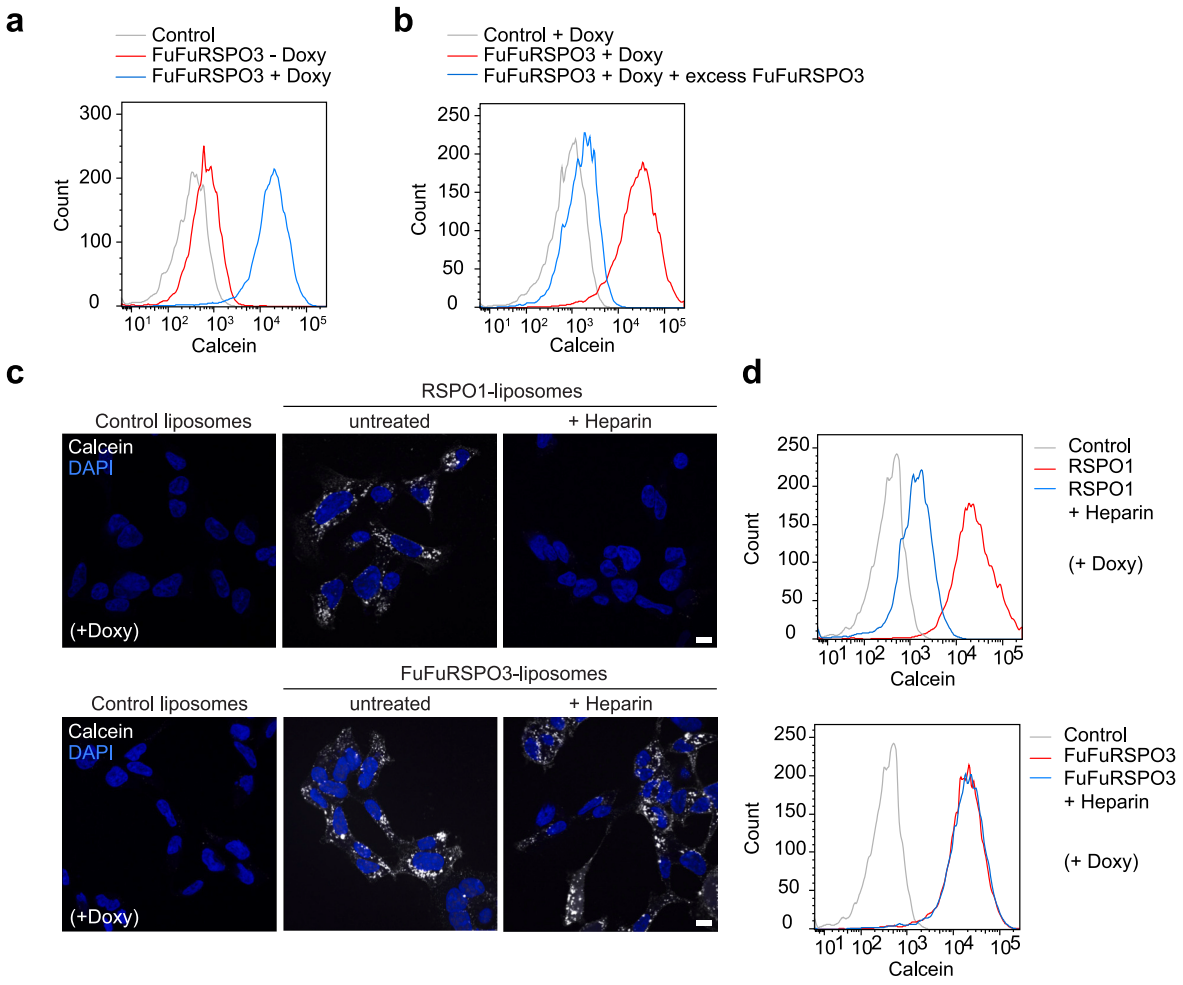

Fig. 4. FuFuRSPO3-liposomes can specifically detect LGR-positive cells. (a) Uptake of FuFuRSPO3-liposomes is enhanced upon overexpression of LGR5. FACS plots showing a 3 h uptake of calcein-labeled FuFuRSPO3-liposomes in control (-Doxy) and LGR5-overexpressing (+Doxy) HEK293T cells. (b) Uptake of FuFuRSPO3-liposomes in LGR5-expressing cells can be competed with purified FuFuRSPO3. FACS plots showing a 3 h uptake of calcein-labeled FuFuRSPO3-liposomes in HEK293T overexpressing LGR5 (+Doxy) in the presence or absence of 60-fold excess purified FuFuRSPO3. (c,d) In contrast to RSPO1, the uptake of FuFuRSPO3-liposomes in LGR5-expressing cells cannot be competed with heparin. Confocal images (c) and FACS plots (d) showing a 3 h uptake of calcein-labeled RSPO1- and FuFuRSPO3-liposomes in HEK293T overexpressing LGR5 in the presence or absence of heparin (0,5 mg/mL). Scale bars, 10 μm.

nucleus (Fig. 5a). After a 24 h chase period, endosomal fluorescence was gradually lost while nuclear signals accumulated, indicating that doxorubicin redistributed from endosomes to the nucleus (Fig. 5a). By contrast, treatment of cells with control doxorubicin-loaded DPPC liposomes only revealed low amounts of nuclear fluorescence after 3 h of incubation, with a loss of detectable signal after a 24 h chase (Fig. 5a).

To demonstrate that endosomal uptake of FuFuRSPO3-liposomes is mediated by LGR5, we labeled the cell surface localized SNAP-tagged LGR5 using SNAP-surface-Alexa^{549} for 15 min [63]. Subsequent incubation with doxorubicin-loaded FuFuRSPO3-liposomes for 3 h revealed a clear colocalization of LGR5 and doxorubicin within endosomal compartments (Fig. 5b), while control liposomes did not show any endosomal fluorescence (Fig. 5b). We conclude that FuFuRSPO3-liposomes are selectively taken up by target cells via LGR5-mediated endocytosis. Subsequently, doxorubicin is released from endosomal compartments and accumulates in the nucleus of target cells.

To assess the capacity of drug-loaded FuFuRSPO3-liposomes to eliminate LGR5-expressing cells, we treated doxycycline-induced LGR5-expressing and uninduced HEK293T cells for 3 h with control or FuFuRSPO3-liposomes carrying increasing dosages of doxorubicin. Indeed, colony formation assays performed after 6 days revealed that treatment with FuFuRSPO3-liposomes, but not control liposomes, selectively prevented the outgrowth of LGR5-expressing cells (Fig. 5c).

These results argue that FuFuRSPO3-liposomes selectively bind LGR5, which mediates their cellular entry via endocytosis. Subsequently, doxorubicin content is released from endosomal compartments and accumulates in the nucleus. The resulting DNA damage and inhibition of replication is thus capable of selectively killing LGR5-high expressing cells.

LGR5-high expressing cells are associated with the initiation and progression of colorectal cancer [33,64]. To examine if LGR5-high cancer cells are sensitive to targeting by FuFuRSPO3-liposomes, we employed two LGR5-high cancer cell lines, Huh7 (hepatocellular carcinoma) and LoVo (colorectal cancer). We confirmed that LGR5 expression in both lines was strongly increased relative to HEK293T cells (Fig. S5b). In line with this observation, FuFuRSPO3-liposomes displayed an increased capacity to deliver doxorubicin to Huh7 cells as compared to control liposomes (Fig. S5c). To assess whether the uptake of doxorubicin-loaded FuFuRSPO3-liposomes is sufficient to interfere with growth, we incubated Huh7 and LoVo cells for 3 h with control or FuFuRSPO3-liposomes using a range of liposomal dilutions. Colony formation assays performed after 5 days revealed that FuFuRSPO3-liposomes consistently displayed enhanced growth-inhibitory capacity for both LGR5-high cancer cell lines as compared to control liposomes (Fig. 5d, e, S5d, S5e).

Truncating mutations in the Wnt/β-catenin pathway tumor

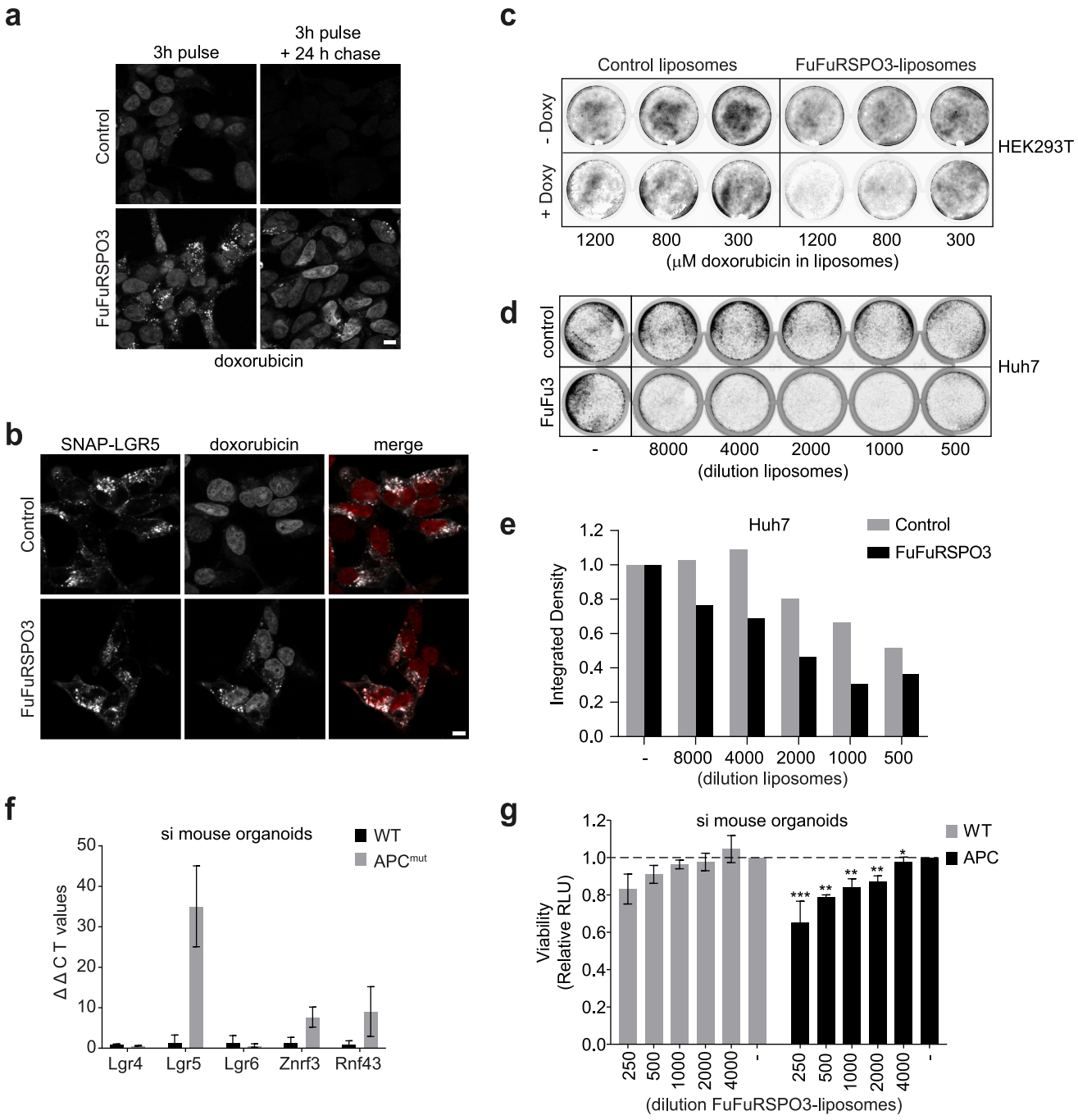

Fig. 5. Doxorubicin-loaded FuFuRSPO3-liposomes can specifically kill LGR5-expressing cells.
(a) Doxorubicin derived from FuFuRSPO3-liposomes is released from endosomal structures and accumulates in the nucleus. Confocal images showing the uptake of doxorubicin-loaded control and FuFuRSPO3-liposomes in LGR5-expressing HEK293T cells. Note the localization of doxorubicin in endosomal structures after a 3 h pulse and the release and accumulation in the nucleus after a 24 h chase. Scale bar, 10 μm. (b) Doxorubicin-loaded FuFuRSPO3-liposomes colocalize with SNAP-LGR5. Confocal images showing the uptake of doxorubicin-loaded FuFuRSPO3-liposomes in SNAP-LGR5-expressing HEK293T. Cells were labeled for 15 min with SNAP-surface-Alexa^{549} and incubated with control or doxorubicin-loaded FuFuRSPO3-liposomes for 3 h. Scale bar, 10 μm. (c) Doxorubicin-loaded FuFuRSPO3-liposomes show increased killing of HEK293T cells overexpressing LGR5 compared to control cells and control liposomes. Colony formation assay in control (-Doxy) and LGR5-expressing (+Doxy) HEK293T cells treated with control and FuFuRSPO3-liposomes loaded with the indicated doxorubicin concentrations. Liposomes were added 1:800 for 3 h and stained after 6 d. (d,e) Doxorubicin-loaded FuFuRSPO3-liposomes show increased killing of Huh7 cells as compared to control liposomes. (d) Colony formation assay in Huh7 cells treated with doxorubicin-loaded control and FuFuRSPO3-liposomes. Cells were treated for 3 h with the indicated liposome dilutions and stained after 6 d. Image (d) and quantification (e) of a representative experiment is shown ($n = 3$). (f) APC-mutant organoids (APC^{mut}) express higher levels of RSPO-binding partners compared to wild-type (WT) small intestinal (si) organoids. Expression values were determined using RT-qPCR. CT values were corrected for housekeeping genes and then corrected for the average expression of all WT samples to create ΔΔCT values +/− SD. (g) APC^{mut} organoids are more sensitive to doxorubicin-loaded FuFuRSPO3-liposomes compared to WT organoids. Organoids were treated with the indicated dilutions of doxorubicin-loaded FuFuRSPO3-liposomes (2722 μM) for 2 h and analysed after 48 h. Graph showing cell viability in relative light units (RLU) corrected for RLU of untreated control organoids of the same genotype +/− SD. *** ($p < 0.001$; ** ($p < 0.01$), * ($p < 0.05$).

suppressor APC comprise a major driver event of colorectal cancer that elevates Wnt signaling and strongly induces expression of the Wnt target gene LGR5 [63]. To assess whether FuFuRSPO3-liposomes preferably target LGR5-high APC-mutant cells (APC^{mut}), we made use of a mouse small intestinal APC^{mut} organoid model. As expected, APC^{mut} organoids express strongly increased levels of *Lgr5* as compared to wild-type organoids (Fig. 5f). Furthermore, the expression of Wnt target genes *Znrf3* and *Rnf43* was also increased in APC^{mut} organoids, together reaching an estimated 53-fold increase in the expression of RSPO-binding partners (Fig. 5f). Next, APC^{mut} and wild-type organoids were pulsed for 2 h with either free doxorubicin or doxorubicin-loaded FuFuRSPO3-liposomes and chased for 2 days. While both organoid lines were equally sensitive to treatment with free doxorubicin (Fig. S5f), APC^{mut} organoids displayed a significantly decreased viability when treated with doxorubicin-loaded FuFuRSPO3 liposomes as compared to wild-type organoids (Fig. 5g). Together, these results indicate that doxorubicin-loaded FuFuRSPO3 liposomes can be employed to selectively target cancer cells that display high levels of LGR5 expression.

4. Discussion

LGR5 provides an attractive putative target for treatment of multiple cancer types, due to its high expression in CSCs [20,28,32,66–68]. Here, we developed and optimized a liposome-based strategy for the targeted delivery of drugs to LGR5 high-expressing cells. To this end, we first decorated liposomes with RSPO1, the natural ligand for members of the LGR family [1–3]. Surprisingly, although the Wnt potentiating activity of RSPO1-liposomes was strictly LGR-dependent, its uptake by cells was largely independent of LGR expression and could be efficiently competed by heparin treatment. Thus, cellular uptake of full-length RSPO1 is predominantly mediated by proteoglycan-binding and does not correlate directly with biological activity. These findings are difficult to reconcile with a previous study in which full-length RSPO1-coupled and doxorubicin-loaded liposomes were employed for the selective targeting of LGR5-positive cancer cells [34]. Remarkably, RSPO1 coupling in this previous study relied on a free Cys present in the N-terminal signal peptide, which would not normally be preserved in the mature, secreted protein. Notwithstanding these differences in liposomal design, our findings strongly argue that proteoglycan binding by the TSP/BR domain, which is conserved across the RSPO family, prevents usage of full-length RSPO for the identification and targeting of LGR5 high-expressing cells.

We were able to overcome LGR-independent uptake of RSPO-coated liposomes by omitting the TSP/BR domain and using the RSPO-derived Fu-domains for liposomal coupling. To achieve this, we employed the Fu-domains of RSPO3 that display preferred binding to LGR5 [1]. Indeed, by using fluorescence-loaded liposomes decorated with FuFuRSPO3 fragments we were able to demonstrate selective uptake of liposomes by LGR5-expressing cells. Furthermore, uptake of FuFuRSPO3-liposomes remained unaffected by heparin treatment and, as fluorescent signals accumulated in endosomal-like structures, we anticipate that uptake primarily takes place via endocytosis.

Finally, we assessed usage of FuFuRSPO3-liposomes for cytotoxic drug delivery. We employed doxorubicin, a broad anticancer compound that is commonly used for liposome-based applications [69]. Our findings indicate that usage of functionalized liposomes to target specific (cancer) cell subsets requires careful optimization. First, although usage of DPPC liposome formulations to a large extent reduced doxorubicin leakage, longer treatments with these liposomes still mediated aspecific cell killing, likely due to continued low levels of leakage. By adapting our treatment schedule, using a shortened liposome incubation time ($2-3h$) followed by a longer chase period (>24 h), we were able to overcome this issue and demonstrated that doxorubicin-loaded FuFuRSPO3-liposomes induce LGR5-specific cytotoxic effects in HEK293T cells overexpressing LGR5. Moreover, our results show that doxorubicin-loaded FuFuRSPO3-liposomes selectively target liver and colorectal cancer cells and APC^{mut} intestinal organoids that express enhanced endogenous levels of LGR5. Mechanistically, the fluorescent properties of doxorubicin allowed us to robustly show that FuFuRSPO3-liposomes delivered their content primarily via LGR5-specific endocytosis, after which doxorubicin was released from endosomes and accumulated in the nucleus to exert cytotoxic effects. By contrast, leakage from control liposomes only resulted in (weak) nuclear fluorescence, indicating that the route of doxorubicin uptake in this case likely occurred in an endocytosis-independent manner. Taken together, our results demonstrate that FuFuRSPO3-decorated liposomes provide promising tools for specific targeting of LGR5-expressing cells, although the type of encapsulated drug will need further adaptation to allow for cellular delivery with highest levels of efficacy.

Of note, while we showed that FuFuRSPO3-liposomes lack affinity for LGR-negative cells, they will likely display affinity for cells that express LGR4 or LGR6 as well [1,70,71]. As LGR4, LGR5 and LGR6 are frequently co-overexpressed in various cancer types, this property may provide an advantage to overcome plasticity effects due to LGR5 downregulation. Indeed, an RSPO4-derived drug-conjugated peptibody that was capable of binding to all three LGRs, displayed promising anti-tumor effects in vivo [72]. In this previous work, a mutant fragment of RSPO4 was used, that allowed for LGR-binding yet failed to induce Wnt pathway potentiating effects [72]. This strategy may prevent adverse effects due to inappropriate Wnt pathway activation in healthy organs, such as intestinal enlargement [73].

In summary, we provide evidence that FuFuRSPO3-coupled liposomes provide a promising strategy to selectively bind and target LGR5 high-expressing cancer stem cells. Optimization of liposome-encapsulated cytotoxic drugs will be required to further enhance efficacy of LGR5-high cell eradication. In future strategies, combination treatment of LGR5 ablation with e.g. EGFR targeting [74,75] or 5-FU [76,77] treatment may provide additional benefits for enhanced therapeutic efficacy.

CRediT authorship contribution statement

Peter van Kerkhof: Investigation, Methodology, Writing – original draft, Writing – review & editing, Formal analysis, Visualization. **Tomica Kralj:** Investigation, Methodology, Formal analysis. **Francesca Spanevello:** Investigation, Methodology, Writing – original draft, Formal analysis, Visualization. **Louis van Bloois:** Investigation, Methodology. **Ingrid Jordens:** Investigation, Methodology, Formal analysis, Writing – original draft, Writing – review & editing, Visualization. **Jelte van der Vaart:** Investigation, Methodology, Formal analysis, Writing – review & editing, Visualization. **Cara Jamieson:** Resources. **Alessandra Merenda:** Writing – original draft. **Enrico Mastrobattista:** Conceptualization, Resources, Writing – review & editing, Supervision, Funding acquisition. **Madelon M. Maurice:** Conceptualization, Writing – original draft, Writing – review & editing, Supervision, Project administration, Funding acquisition.

All authors reviewed the manuscript.

Declaration of Competing Interest

M.M.M is a co-founder and shareholder for LaigoBio, The Netherlands.

Data availability

Data will be made available on request.

Acknowledgments

We thank members of the laboratory of M.M.M. for discussions and suggestions, Dieuwke Marvin for technical assistance and Huiying Ma

for the generation of the mouse small intestinal APC^{mut} organoids. Rajat Rohatgi for the WT and LGR4/5/6 triple knockout HAP1 cells (Beckman center, Stanford). Bruno Reversade for the WT and LGR4/5/6 triple knockout MEF cells (A*STAR, Singapore). Niels de Wind for the LoVo cells (LUMC, Leiden) and Bart Spee for the Huh7 cells (UU, Utrecht). This work is part of the Oncode Institute, which is partly financed by the Dutch Cancer Society. This work was supported by the Netherlands Organization for Scientific Research NWO VICI Grant 91815604, TOP Grant 91218050 (to M.M.M.) and a Seed grant from Utrecht University (to M.M.M. and E.M.).

Appendix A. Supplementary data

Supplementary data to this article can be found online at https://doi.org/10.1016/j.jconrel.2023.02.025.

References

[1] K.S. Carmon, X. Gong, Q. Lin, A. Thomas, Q. Liu, R-spondins function as ligands of the orphan receptors LGR4 and LGR5 to regulate Wnt/β-catenin signaling, Proc. Natl. Acad. Sci. U. S. A. 108 (2011) 11452–11457, https://doi.org/10.1073/pnas.1106083108.

[2] A. Glinka, C. Dolde, N. Kirsch, Y.L. Huang, O. Kazanskaya, D. Ingelfinger, M. Boutros, C.M. Cruciat, C. Niehrs, LGR4 and LGR5 are R-spondin receptors mediating Wnt/β-catenin and Wnt/PCP signalling, EMBO Rep. 12 (2011) 1055–1061, https://doi.org/10.1038/embor.2011.175.

[3] W. De Lau, N. Barker, T.Y. Low, B.K. Koo, V.S.W. Li, H. Teunissen, P. Kujala, A. Haegebarth, P.J. Peters, M. Van De Wetering, D.E. Stange, J. Van Es, D. Guardavaccaro, R.B.M. Schasfoort, Y. Mohri, K. Nishimori, S. Mohammed, A.J. R. Heck, H. Clevers, Lgr5 homologues associate with Wnt receptors and mediate R-spondin signalling, Nature. 476 (2011) 293–297, https://doi.org/10.1038/nature10337.

[4] M. Zebisch, Y. Xu, C. Krastev, B.T. Macdonald, M. Chen, R.J.C. Gilbert, X. He, E.Y. Jones, Structural and molecular basis of ZNRF3/RNF43 transmembrane ubiquitin ligase inhibition by the Wnt agonist R-spondin, Nat. Commun. 4 (2013) 2787, doi: 10.1038/ncomms3787.

[5] P.H. Chen, X. Chen, Z. Lin, D. Fang, X. He, The structural basis of R-spondin recognition by LGR5 and RNF43, Genes Dev. 27 (2013) 1345–1350, https://doi.org/10.1101/gad.219915.113.

[6] W.C. Peng, W. deLau, F. Forneris, J.C.M. Granneman, M. Huch, H. Clevers, P. Gros, Structure of stem cell growth factor R-spondin 1 in complex with the ectodomain of its receptor LGR5, Cell Rep. 3 (2013) 1885–1892, https://doi.org/10.1016/J.CELREP.2013.06.009.

[7] W.C. Peng, W. De Lau, P.K. Madoori, F. Forneris, J.C.M. Granneman, H. Clevers, P. Gros, Structures of Wnt-antagonist ZNRF3 and its complex with R-spondin 1 and implications for signaling, PLoS One 8 (2013) 1–10, https://doi.org/10.1371/journal.pone.0083110.

[8] M. Zebisch, E.Y. Jones, Crystal structure of R-spondin 2 in complex with the ectodomains of its receptors LGR5 and ZNRF3, J. Struct. Biol. 191 (2015) 149–155, https://doi.org/10.1016/J.JSB.2015.05.008.

[9] W.B.M. de Lau, B. Snel, H.C. Clevers, The R-spondin protein family, Genome Biol. 13 (2012) 242, https://doi.org/10.1186/GB-2012-13-3-242.

[11] W.C. Peng, W. De Lau, P.K. Madoori, F. Forneris, J.C.M. Granneman, H. Clevers, P. Gros, Structures of Wnt-antagonist ZNRF3 and its complex with R-Spondin 1 and implications for signaling, PLoS One 8 (2013), e83110, https://doi.org/10.1371/JOURNAL.PONE.0083110.

[12] M. Zebisch, E.Y. Jones, Crystal structure of R-spondin 2 in complex with the ectodomains of its receptors LGR5 and ZNRF3, J. Struct. Biol. 191 (2015) 149–155, https://doi.org/10.1016/j.jsb.2015.05.008.

[13] H. Chen, J. Sottile, D.K. Strickland, D.F. Mosher, Binding and degradation of thrombospondin-1 mediated through heparan sulphate proteoglycans and low-density-lipoprotein receptor-related protein : localization of the functional activity to the trimeric N-terminal heparin-binding region of thrombospondin-1, Biochem. J. 318 (1996) 959–963, https://doi.org/10.1042/bj3180959.

[14] B. Ohkawara, A. Glinka, C. Niehrs, Rspo3 binds syndecan 4 and induces Wnt/PCP signaling via clathrin-mediated endocytosis to promote morphogenesis, Dev. Cell 20 (2011) 303–314, https://doi.org/10.1016/J.DEVCEL.2011.01.006.

[15] L. Ayadi, Molecular modelling of the TSR domain of R-spondin 4, Bioinformation. 3 (2008) 119–123, https://doi.org/10.6026/97320630003119.

[16] G. Van Schoore, F. Mendive, R. Pochet, G. Vassart, Expression pattern of the orphan receptor LGR4/GPR48 gene in the mouse, Histochem. Cell Biol. 124 (2005) 35–50, https://doi.org/10.1007/S00418-005-0002-3.

[17] H.J. Snippert, A. Haegebarth, M. Kasper, V. Jaks, J.H. Van Es, N. Barker, M. Van De Wetering, M. Van Den Born, H. Begthel, R.G. Vries, D.E. Stange, R. Toftgård, H. Clevers, Lgr6 marks stem cells in the hair follicle that generate all cell lineages of the skin, Science. 327 (2010) 1385–1389, https://doi.org/10.1126/SCIENCE.1184733.

[18] A. Füllgrabe, S. Joost, A. Are, T. Jacob, U. Sivan, A. Haegebarth, S. Linnarsson, B. D. Simons, H. Clevers, R. Toftgård, M. Kasper, Dynamics of Lgr6+ progenitor cells in the hair follicle, sebaceous gland, and interfollicular epidermis, Stem Cell Rep. 5 (2015) 843–855, https://doi.org/10.1016/J.STEMCR.2015.09.013.

[19] N. Barker, H. Clevers, Leucine-rich repeat-containing G-protein-coupled receptors as markers of adult stem cells, Gastroenterology. 138 (2010) 1681–1696, https://doi.org/10.1053/J.GASTRO.2010.03.002.

[20] N. Barker, J.H. Van Es, J. Kuipers, P. Kujala, M. Van Den Born, M. Cozijnsen, A. Haegebarth, J. Korving, H. Begthel, P.J. Peters, H. Clevers, Identification of Stem Cells in Small Intestine and colon by Marker Gene Lgr5, Nature 449 (2007) 1003–1007, https://doi.org/10.1038/nature06196.

[21] W. Liu, J. Zhang, X. Gan, F. Shen, X. Yang, N. Du, D. Xia, L. Liu, L. Qiao, J. Pan, Y. Sun, X. Xi, LGR5 promotes epithelial ovarian cancer proliferation, metastasis, and epithelial–mesenchymal transition through the Notch1 signaling pathway, Cancer Med. 7 (2018) 3132–3142, https://doi.org/10.1002/CAM4.1485.

[22] Y. Yamamoto, M. Sakamoto, G. Fujii, H. Tsuiji, K. Kanetaka, M. Asaka, S. Hirohashi, Overexpression of orphan G-protein–coupled receptor, Gpr49, in human hepatocellular carcinomas with β-catenin mutations, Hepatology. 37 (2003) 528–533, https://doi.org/10.1053/JHEP.2003.50029.

[23] J. Yi, W. Xiong, X. Gong, S. Bellister, L.M. Ellis, Analysis of LGR4 receptor distribution in human and mouse tissues, PLoS One 8 (2013) 78144, https://doi.org/10.1371/journal.pone.0078144.

[24] M.R. Junttila, W. Mao, X. Wang, B.E. Wang, T. Pham, J. Flygare, S.F. Yu, S. Yee, D. Goldenberg, C. Fields, J. Eastham-Anderson, M. Singh, R. Vij, J.A. Hongo, R. Firestein, M. Schutten, K. Flagella, P. Polakis, A.G. Polson, Targeting LGR5+ cells with an antibody-drug conjugate for the treatment of colon cancer, Sci. Transl. Med. 7 (2015) 314ra186, doi:10.1126/SCITRANSLMED.AAC7433.

[25] T. McClanahan, S. Koseoglu, K. Smith, J. Grein, E. Gustafson, S. Black, P. Kirschmeier, A.A. Samatar, Identification of overexpression of orphan G protein-coupled receptor GPR49 in human colon and ovarian primary tumors, Cancer Biol Ther. 5 (2006) 419–426, https://doi.org/10.4161/CBT.5.4.2521.

[26] R.G. Morgan, E. Mortensson, A.C. Williams, Targeting LGR5 in colorectal cancer: therapeutic gold or too plastic? Br. J. Cancer 118 (2018) 1410–1418, https://doi.org/10.1038/s41416-018-0118-6.

[27] A.G. Schepers, H.J. Snippert, D.E. Stange, M. van den Born, J.H. van Es, M. van de Wetering, H. Clevers, Lineage tracing reveals Lgr5+ stem cell activity in mouse intestinal adenomas, Science. 337 (2012) 730–735, https://doi.org/10.1126/science.1224676.

[28] F. De Sousa, E. Melo, A.V. Kurtova, J.M. Harnoss, N. Kljavin, J.D. Hoeck, J. Hung, J.E. Anderson, E.E. Storm, Z. Modrusan, H. Koeppen, G.J.P. Dijkgraaf, R. Piskol, F. J. De Sauvage, A distinct role for Lgr5 + stem cells in primary and metastatic colon cancer, Nature 543 (2017) 676–680, https://doi.org/10.1038/nature21713.

[29] F.-J. Gao, J.-Y. Chen, H.-Y. Wu, J. Shi, M. Chen, X.-S. Fan, Q. Huang, Lgr5 over-expression is positively related to the tumor progression and HER2 expression in stage pTNM IV colorectal cancer, Int. J. Clin. Exp. Pathol. 7 (2014) 1572–1579.

[30] M.-F. Hou, P.-M. Chen, P.-Y. Chu, LGR5 overexpression confers poor relapse-free survival in breast cancer patients, BMC Cancer 18 (2018) 219, https://doi.org/10.1186/s12885-018-4018-1.

[31] A. Merlos-Suárez, F.M. Barriga, P. Jung, M. Iglesias, M.V. Céspedes, D. Rossell, M. Sevillano, X. Hernando-Momblona, V. Da Silva-Diz, P. Muñoz, H. Clevers, E. Sancho, R. Mangues, E. Batlle, The intestinal stem cell signature identifies colorectal cancer stem cells and predicts disease relapse, Cell Stem Cell 8 (2011) 511–524, https://doi.org/10.1016/J.STEM.2011.02.020.

[32] A. Fumagalli, K.C. Oost, J.E. Suijkerbuijk, H.J. Snippert, J. Van, R. Correspondence, Plasticity of Lgr5-negative cancer cells drives metastasis in colorectal cancer, Cell Stem Cell 26 (2020) 569–578, https://doi.org/10.1016/j.stem.2020.02.008.

[33] M. Shimokawa, Y. Ohta, S. Nishikori, M. Matano, A. Takano, M. Fujii, S. Date, S. Sugimoto, T. Kanai, T. Sato, Visualization and targeting of LGR5 + human colon cancer stem cells, Nature. 545 (2017) 187–192, https://doi.org/10.1038/nature22081.

[34] J. Cao, C. Li, X. Wei, M. Tu, Y. Zhang, F. Xu, Y. Xu, Selective targeting and eradication of LGR5 + cancer stem cells using RSPO-conjugated doxorubicin liposomes, Mol. Cancer Ther. 17 (2018) 1475–1485, https://doi.org/10.1158/1535-7163.MCT-17-0694.

[35] X. Gong, A. Azhdarinia, S.C. Ghosh, W. Xiong, Z. An, Q. Liu, K.S. Carmon, LGR5-targeted antibody-drug conjugate eradicates gastrointestinal tumors and prevents recurrence, Mol. Cancer Ther. 15 (2016) 1580–1590, https://doi.org/10.1158/1535-7163.MCT-16-0114.

[36] T.M. Allen, P.R. Cullis, Liposomal drug delivery systems: from concept to clinical applications, Adv. Drug Deliv. Rev. 65 (2013) 36–48, https://doi.org/10.1016/J.ADDR.2012.09.037.

[37] A.S. Ulrich, Biophysical aspects of using liposomes as delivery vehicles, Biosci. Rep. 22 (2002) 129–150, https://doi.org/10.1023/A:1020178304031.

[38] L. Sercombe, T. Veerati, F. Moheimani, S.Y. Wu, A.K. Sood, S. Hua, Advances and challenges of liposome assisted drug delivery, Front. Pharmacol. 6 (2015) 1–13, https://doi.org/10.3389/fphar.2015.00286.

[39] M. Li, C. Du, N. Guo, Y. Teng, X. Meng, H. Sun, S. Li, P. Yu, H. Galons, Composition design and medical application of liposomes, Eur. J. Med. Chem. 164 (2019) 640–653, https://doi.org/10.1016/J.EJMECH.2019.01.007.

[40] P. Sapra, P. Tyagi, T. Allen, Ligand-targeted liposomes for cancer treatment, Curr. Drug Deliv. 2 (2005) 369–381, https://doi.org/10.2174/156720105774370159.

[41] S. Sarrazin, W.C. Lamanna, J.D. Esko, Heparan sulfate proteoglycans, Cold Spring Harb. Perspect. Biol. 3 (2011), https://doi.org/10.1101/cshperspect.a004952.

[42] D.V.F. Tauriello, I. Jordens, K. Kirchner, J.W. Slootstra, T. Kruitwagen, B.A. M. Bouwman, M. Noutsou, S.G.D. Rüdiger, K. Schwamborn, A. Schambony, M. M. Maurice, Wnt/β-catenin signaling requires interaction of the Dishevelled DEP domain and C terminus with a discontinuous motif in frizzled, Proc. Natl. Acad. Sci. U. S. A. 109 (2012), https://doi.org/10.1073/pnas.1114802109.

[43] D.V.F. Tauriello, A. Haegebarth, I. Kuper, M.J. Edelmann, M. Henraat, M. R. Canninga-van Dijk, B.M. Kessler, H. Clevers, M.M. Maurice, Loss of the tumor

suppressor CYLD enhances Wnt/β-catenin signaling through K63-linked ubiquitination of Dvl, Mol. Cell 37 (2010) 607–619, https://doi.org/10.1016/J.MOLCEL.2010.01.035.
[44] N. Fenderico, R.C. van Scherpenzeel, M. Goldflam, D. Proverbio, I. Jordens, T. Kralj, S. Stryeck, T.Z. Bass, G. Hermans, C. Ullman, T. Aastrup, P. Gros, M. M. Maurice, Anti-LRP5/6 VHHs promote differentiation of Wnt-hypersensitive intestinal stem cells, Nat. Commun. 10 (2019) 365, https://doi.org/10.1038/s41467-018-08172-z.
[45] F. Olson, C.A. Hunt, F.C. Szoka, W.J. Vail, D. Papahadjopoulos, Preparation of liposomes of defined size distribution by extrusion through polycarbonate membranes, BBA - Biomembr. 557 (1979) 9–23, https://doi.org/10.1016/0005-2736(79)90085-3.
[46] G. Haran, R. Cohen, L.K. Bar, Y. Barenholz, Transmembrane ammonium sulfate gradients in liposomes produce efficient and stable entrapment of amphipathic weak bases, BBA - Biomembr. 1151 (1993) 201–215, https://doi.org/10.1016/0005-2736(93)90105-9.
[47] G. Rouser, S. Fleischer, A. Yamamoto, Two dimensional thin layer chromatographic separation of polar lipids and determination of phospholipids by phosphorus analysis of spots, Lipids. 5 (1970) 494–496, https://doi.org/10.1007/BF02531316.
[48] N. Zhang, A.F. Palmer, Liposomes surface conjugated with human hemoglobin target delivery to macrophages, Biotechnol. Bioeng. 109 (2012) 823–829, https://doi.org/10.1002/BIT.24340.
[49] C.Y. Janda, L.T. Dang, C. You, J. Chang, W. de Lau, Z.A. Zhong, K.S. Yan, O. Marecic, D. Siepe, X. Li, J.D. Moody, B.O. Williams, H. Clevers, J. Piehler, D. Baker, C.J. Kuo, K.C. Garcia, Surrogate Wnt agonists that phenocopy canonical Wnt and β-catenin signalling, Nature. 545 (2017) 234–237, https://doi.org/10.1038/nature22306.
[50] G. Blume, G. Cevc, M.D.J.A. Crommelin, I.A.J.M. Bakker-Woudenberg, C. Kluft, G. Storm, Specific targeting with poly(ethylene glycol)-modified liposomes: coupling of homing devices to the ends of the polymeric chains combines effective target binding with long circulation times, Biochim. Biophys. Acta Biomembr. 1149 (1993) 180–184, https://doi.org/10.1016/0005-2736(93)90039-3.
[51] D. Kirpotin, J.W. Park, K. Hong, S. Zalipsky, W.-L. Li, P. Carter, C.C. Benz, D. Papahadjopoulos, Sterically Stabilized Anti-HER2 Immunoliposomes: Design and Targeting to Human Breast Cancer Cells In Vitro †, Biochemistry 36 (1997) 66–75, https://doi.org/10.1021/bi962148u.
[52] P.E. Saw, S. Kim, I. Lee, J. Park, M. Yu, J. Lee, J.-I. Kim, S. Jon, Aptide-conjugated liposome targeting tumor-associated fibronectin for glioma therapy, J. Mater. Chem. B 1 (2013) 4723–4726, https://doi.org/10.1039/C3TB20815J.
[53] K. Tan, M. Duquette, J.H. Liu, Y. Dong, R. Zhang, A. Joachimiak, J. Lawler, J. H. Wang, Crystal structure of the TSP-1 type 1 repeats a novel layered fold and its biological implication, J. Cell Biol. 159 (2002) 373–382, https://doi.org/10.1083/JCB.200206062.
[54] T.M. Allen, L.G. Cleland, Serum-induced leakage of liposome contents, BBA - Biomembr. 597 (1980) 418–426, https://doi.org/10.1016/0005-2736(80)90118-2.
[55] E. Mastrobattista, G. Storm, L. Van Bloois, R. Reszka, P.G.M. Bloemen, D.J. A. Crommelin, P.A.J. Henricks, Cellular uptake of liposomes targeted to intercellular adhesion molecule-1 (ICAM-1) on bronchial epithelial cells, Biochim. Biophys. Acta Biomembr. 1419 (1999) 353–363, https://doi.org/10.1016/S0005-2736(99)00074-7.
[56] V. Korinek, N. Barker, P.J. Morin, D. Van Wichen, R. De Weger, K.W. Kinzler, B. Vogelstein, H. Clevers, Constitutive transcriptional activation by a β-catenin-Tcf complex in APC(−/−) colon carcinoma, Science. 275 (1997) 1784–1787, https://doi.org/10.1126/SCIENCE.275.5307.1784.
[57] A.M. Lebensohn, R. Rohatgi, R-spondins can potentiate WNT signaling without LGRs, ELife. 7 (2018), https://doi.org/10.7554/ELIFE.33126.
[58] R. Dubey, P. Van Kerkhof, I. Jordens, T. Malinauskas, G.V. Pusapati, J.K. Mckenna, D. Li, J.E. Carette, M. Ho, C. Siebold, M. Maurice, A.M. Lebensohn, R. Rohatgi, R-spondins engage heparan sulfate proteoglycans to potentiate WNT signaling, 2020, pp. 1–24, https://doi.org/10.7554/eLife.54469.
[59] M.K. Kauffman, M.E. Kauffman, H. Zhu, Z. Jia, Y.R. Li, Fluorescence-based assays for measuring doxorubicin in biological systems, React Oxyg Species Apex. 2 (2016) 432–439, https://doi.org/10.20455/ros.2016.873.
[60] Y. Zhao, J.P. May, I.-W. Chen, E. Undzys, S.-D. Li, A Study of Liposomal Formulations to Improve the Delivery of Aquated Cisplatin to a Multidrug Resistant Tumor, Pharm Res. 32 (2015) 3261–3268, https://doi.org/10.1007/s11095-015-1702-6.
[61] G.J.R. Charrois, T.M. Allen, Drug release rate influences the pharmacokinetics, biodistribution, therapeutic activity, and toxicity of pegylated liposomal doxorubicin formulations in murine breast cancer, Biochim. Biophys. Acta Biomembr. 1663 (2004) 167–177, https://doi.org/10.1016/J.BBAMEM.2004.03.006.
[62] S.A. Abraham, D.N. Waterhouse, L.D. Mayer, P.R. Cullis, T.D. Madden, M.B. Bally, The liposomal formulation of doxorubicin, Methods Enzymol. 391 (2005) 71–97, https://doi.org/10.1016/S0076-6879(05)91004-5.
[63] B.K. Koo, M. Spit, I. Jordens, T.Y. Low, D.E. Stange, M. Van De Wetering, J.H. Van Es, S. Mohammed, A.J.R. Heck, M.M. Maurice, H. Clevers, Tumour suppressor RNF43 is a stem-cell E3 ligase that induces endocytosis of Wnt receptors, Nature 488 (2012) 665–669, https://doi.org/10.1038/nature11308.
[64] F. De Sousa, E. Melo, A.V. Kurtova, J.M. Harnoss, N. Kljavin, J.D. Hoeck, J. Hung, J.E. Anderson, E.E. Storm, Z. Modrusan, H. Koeppen, G.J.P. Dijkgraaf, R. Piskol, F. J. De Sauvage, A distinct role for Lgr5 + stem cells in primary and metastatic colon cancer, Nature. 543 (2017) 676–680, https://doi.org/10.1038/nature21713.
[66] L. Vermeulen, M. Todaro, F. De Sousa Mello, M.R. Sprick, K. Kemper, M. Perez Alea, D.J. Richel, G. Stassi, J.P. Medema, Single-cell cloning of colon cancer stem cells reveals a multi-lineage differentiation capacity, Proc. Natl. Acad. Sci. U. S. A. 105 (2008) 13427–13432, https://doi.org/10.1073/PNAS.0805706105.
[67] K. Kemper, P.R. Prasetyanti, W. De Lau, H. Rodermond, H. Clevers, J.P. Medema, Monoclonal antibodies against Lgr5 identify human colorectal cancer stem cells, Stem Cells 30 (2012) 2378–2386, https://doi.org/10.1002/STEM.1233.
[68] S. Kobayashi, H. Yamada-Okabe, M. Suzuki, O. Natori, A. Kato, K. Matsubara, Y. J. Chen, M. Yamazaki, S. Funahashi, K. Yoshida, E. Hashimoto, Y. Watanabe, H. Mutoh, M. Ashihara, C. Kato, T. Watanabe, T. Yoshikubo, N. Tamaoki, T. Ochiya, M. Kuroda, A.J. Levine, T. Yamazaki, LGR5-positive colon cancer stem cells interconvert with drug-resistant LGR5-negative cells and are capable of tumor reconstitution, Stem Cells. 30 (2012) 2631–2644, https://doi.org/10.1002/STEM.1257.
[69] V. Makwana, J. Karanjia, T. Haselhorst, S. Anoopkumar-Dukie, S. Rudrawar, Liposomal doxorubicin as targeted delivery platform: current trends in surface functionalization, Int. J. Pharm. 593 (2021), 120117, doi:10.1016/J.IJPHARM.2020.120117.
[70] H.E. Moad, A.A. Pioszak, Reconstitution of R-Spondin:LGR4:ZNRF3 Adult Stem Cell Growth Factor Signaling Complexes with Recombinant Proteins Produced in *Escherichia coli*, Biochemistry 52 (2013) 7295–7304, https://doi.org/10.1021/bi401090h.
[71] M.L. Warner, T. Bell, A.A. Pioszak, Engineering high-potency R-spondin adult stem cell growth factors, Mol. Pharmacol. 87 (2015) 410–420, https://doi.org/10.1124/MOL.114.095133.
[72] J. Cui, Y. Toh, S. Park, W. Yu, J. Tu, L. Wu, L. Li, J. Jacob, S. Pan, K.S. Carmon, Q. J. Liu, Drug conjugates of antagonistic R-Spondin 4 mutant for simultaneous targeting of leucine-rich repeat-containing G protein-coupled receptors 4/5/6 for Cancer treatment, J. Med. Chem. 64 (2021) 12572–12581, https://doi.org/10.1021/acs.jmedchem.1c00395.
[73] K.A. Kim, M. Kakitani, J. Zhao, T. Oshima, T. Tang, M. Binnerts, Y. Liu, B. Boyle, E. Park, P. Emtage, W.D. Funk, K. Tomizuka, Medicine: mitogenic influence of human R-spondin1 on the intestinal epithelium, Science. 309 (2005) 1256–1259, https://doi.org/10.1126/SCIENCE.1112521.
[74] C.L. Arteaga, J.A. Engelman, ERBB receptors: from oncogene discovery to basic science to mechanism-based cancer therapeutics, Cancer Cell 25 (2014) 282–303, https://doi.org/10.1016/J.CCR.2014.02.025.
[75] S. Guardiola, M. Varese, M. Sánchez-Navarro, E. Giralt, A third shot at EGFR: new opportunities in cancer therapy, Trends Pharmacol. Sci. 40 (2019) 941–955, https://doi.org/10.1016/J.TIPS.2019.10.004.
[76] D.B. Longley, D.P. Harkin, P.G. Johnston, 5-Fluorouracil: Mechanisms of Action and Clinical Strategies, Nat. Rev. Cancer 3 (2003) 330–338, https://doi.org/10.1038/nrc1074.
[77] S. Vodenkova, T. Buchler, K. Cervena, V. Veskrnova, P. Vodicka, V. Vymetalkova, 5-fluorouracil and other fluoropyrimidines in colorectal cancer: past, present and future, Pharmacol. Ther. 206 (2020) 107447, https://doi.org/10.1016/J.PHARMTHERA.2019.107447.